Mineralogy and Petrology (2020) 114:319–327
https://doi.org/10.1007/s00710-020-00702-2

ORIGINAL PAPER

Stergiouite, $CaZn_2(AsO_4)_2 \cdot 4H_2O$ – a new mineral from the Lavrion Mining District, Greece

Branko Rieck[1] · Gerald Giester[1] · Christian L. Lengauer[1] · Chutimun Chanmuang N.[1] · Dan Topa[2]

Received: 4 November 2019 / Accepted: 25 February 2020 / Published online: 3 April 2020

Abstract

Stergiouite is a new mineral from the Plaka area in the northern part of the Lavrion Mining District, Greece. The mineral occurs as clusters of stacked, platy crystals, associated with galena, sphalerite, native arsenic and sulfur. The crystals are white to colorless, with a pearly luster and white streak. No luminescence under ultraviolet (UV) radiation is observed. Stergiouite is brittle and has a Mohs hardness of ~3. Chemical analysis gave As_2O_5 42.93 wt%; Sb_2O_5 2.45 wt%; CaO 10.90 wt%; ZnO 29.79 wt%; and H_2O_{calc} 13.93 wt%, which corresponds to an empirical formula $Ca_{1.02}Zn_{1.91}((As_{0.95}Sb_{0.08})O_4)_{\Sigma 2.03} \cdot 4H_2O$. The ideal formula is $CaZn_2(AsO_4)_2 \cdot 4H_2O$. Stergiouite is monoclinic, space group *Pc*, with unit-cell parameters *a* 9.416(2) Å; *b* 5.300(1) Å; *c* 10.893(2) Å; β 91.767(10)°; *V* 543.36(3) Å^3; $Z = 2$. The strongest lines in the Gandolfi X-ray powder pattern [*d* in Å, I/I_{100}, (*hkl*)] are: 9.406, 100, (100); 4.619, 80, (102), (110); 3.612, 35, $(20\bar{2})$; 3.494, 35, (112); 2.984, 60, $(21\bar{2})$; 2.922, 50, (212); 2.720, 20, (004); and 2.647, 25, (020). The crystal structure was refined based on single-crystal X-ray diffraction data to $R1 = 0.046$, $wR2 = 0.093$. The observed mass density of 3.1(2) g cm^{-3} compares well with the calculated value (3.183 g cm^{-3}). The framework structure of stergiouite is built up by one type of $CaO_2(H_2O)_4$ octahedron and each two ZnO_4 and AsO_4 tetrahedra. These polyhedra share common corners to form three- and four-membered rings. A system of hydrogen bonds (O–O range: 2.70–3.02 Å) further stabilizes the structure. The crystal structure of stergiouite is closely related to that of phosphophyllite $[Fe^{[6]}Zn_2^{[4]}(PO_4)_2 \cdot 4H_2O]$ as well as with members of the hopeite $[Zn^{[6]}Zn_2^{[4]}(PO_4)_2 \cdot 4H_2O]$ group. Stergiouite is named in honour of Vasilis Stergiou (born 1958) in recognition of his contributions to the mineralogy of the Lavrion deposits.

Keywords Stergiouite · New mineral · Arsenate · Hopeite group · Lavrion Mining District · Greece

Introduction

The Lavrion Mining District, Attikí Prefecture, Greece, is famous for its lead-zinc-silver-ores that were already mined in ancient times with the earliest proven workings at around 3000 BC. The first peak occurred 600–300 B.C., contributing to the wealth of Athens during the classical period and making much of its successes possible. After a period of diminished importance and even dormancy the mining reopened in 1865 and continued for over a century. Conophagos (1980) estimated that until the depletion and closure of the mines 2.3 Mt of Pb and 7800 t of Au were extracted from the ores.

The Lavrion Mining District is located at the southern tip of the Attika peninsula and spreads over an area of approximately 150 km^2. The area is part of the Attic-Cycladic-Pelagonian ore belt and includes significant "base- and precious metal" deposits located in southern Evia, Sifnos, Tinos and Kythnos (Vavelidis 1997; Skarpelis 2002; Tombros et al. 2004; Neubauer 2005; Tombros et al. 2007). Voudouris (2005) reports several types of sulphide mineralisations in the area including skarn, skarn-free carbonate-replacement and "vein type" ores.

The area is known for the occurrence of about 600 mineral species of which more than 20 are "type locality" minerals. The Lavrion Mining District has been subject to intense investigations by the authors for more than two decades (Rieck 1999; Rieck and Rieck 1999; Rieck and Wendel 1999; Wendel and Rieck 1999a, 1999b; Giester et al. 2000; Giester et al. 2007; Rieck 2012; Giester and Rieck 2014; Kolitsch

Editorial handling: N. V. Chukanov

✉ Gerald Giester
gerald.giester@univie.ac.at

[1] Institut für Mineralogie und Kristallographie, Universität Wien, Althanstr. 14, A–1090 Wien, Austria

[2] Natural History Museum Vienna, Burgring 7, A–1010 Wien, Austria

Fig. 1 The vein with massive native arsenic, sphalerite and galenite that yielded the new mineral stergiouite in situ in the Plaka #80 mine

et al. 2014a, 2014b; Kolitsch et al. 2015; Rieck et al. 2018). Several new mineral species have been described by our research group so far, i.e. mereiterite [$K_2Fe^{2+}(SO_4)_2 \cdot 4H_2O$; Giester and Rieck 1995], niedermayrite [$Cu_4Cd(SO_4)_2(OH)_6 \cdot 4H_2O$; Giester et al. 1998], kapellasite [$Cu_3Zn(OH)_6Cl_2$; Krause et al. 2006], voudourisite [$Cd(SO_4)\cdot H_2O$] and lazaridisite [$Cd_3(SO_4)_3 \cdot 8H_2O$; Rieck et al. 2019], and a new secondary zinc mineral with the formula $Zn_9(SO_4)_2(OH)_{12}Cl_2 \cdot 6H_2O$ (Kolitsch and Giester 2013).

The area of Plaka in the northern part of the Lavrion Mining District is known for relatively fresh vein-type mineralizations (Voudouris 2005), consisting of galena-sphalerite ores with massive banded native arsenic and admixed silver minerals. One such ore shoot was noticed because of its overabundance of native arsenic (see Fig. 1). In open cavities, the arsenic was covered by a thin, amorphous film with noticeable shrinkage and accompanied with native sulfur. Grown on this film were white, platy aggregates which turned out to be the new mineral stergiouite.

Stergiouite is named in honour of Vasilis Stergiou (born on October 30, 1958), in recognition of his recent contributions to the mineralogy of the Lavrion deposits (e.g., Chukanov et al. 2018). The mineral and name have been approved by the Commission on New Minerals, Nomenclature and Classification of the International Mineralogical Association under number IMA 2018-051a. The type material is deposited in the collection of the Natural History Museum Vienna, Austria, with inventory number O 342.

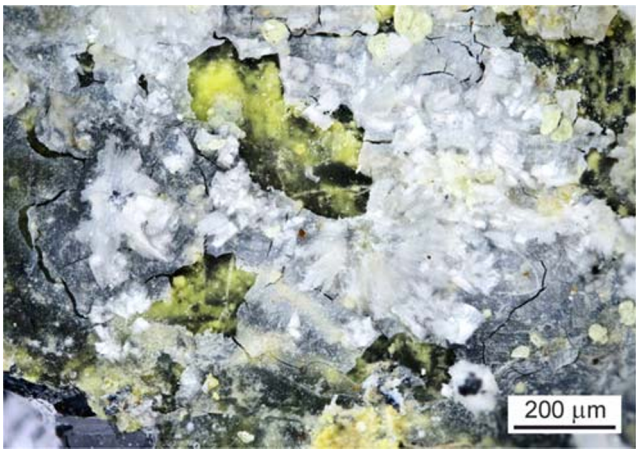

Fig. 2 Stergiouite as white, platy aggregates grown on a thin, amorphous film with noticeable shrinkage and accompanied with native sulfur. The matrix consists of massive native As

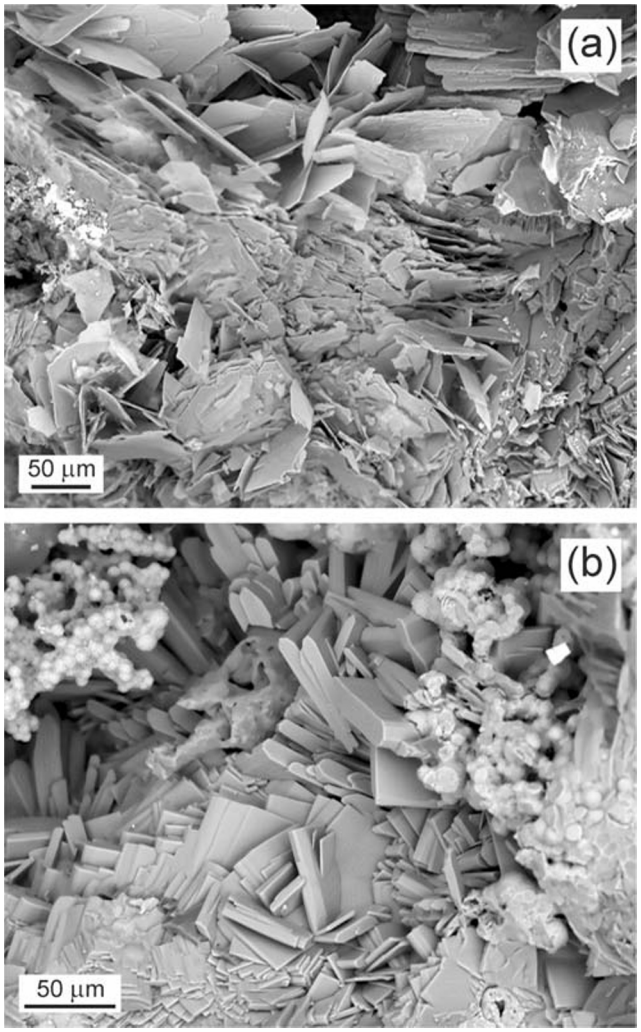

Fig. 3 Secondary electron images of stergiouite. **a** The mineral most commonly forms hypidiomorphic thin plates. **b** Only occasionally well-developed euhedral crystals are observed

General description and analytical characterization

Occurrence

Stergiouite occurs in veins (Fig. 1) that were exposed in the Plaka #80 and Plaka #145 mines. The locality can be reached through the Plaka #80 mine which is deemed the type locality for this mineral. The paragenesis of the new mineral consists of a matrix formed by brecciated galena-sphalerite ores with admixed silver minerals and massive

Table 1 X-ray powder diffraction data (d in Å) for stergiouite

I/I_{100}	I_{cal}	d_{obs}	d_{calc}	h	k	l
100	100	9.406	9.40710	1	0	0
5	13	4.769	4.77514	1	0	–2
80	27	4.619	4.64836	1	0	2
	44	4.619	4.61637	1	1	0
5	4	4.271	4.27334	1	1	–1
1	2	4.228	4.22680	1	1	1
1	2	3.793	3.79616	0	1	2
35	38	3.612	3.61446	2	0	–2
35	20	3.494	3.49418	1	1	2
1	4	3.369	3.36995	2	1	–1
1	3	3.134	3.13570	3	0	0
60	34	2.984	2.98583	2	1	–2
50	53	2.922	2.92330	2	1	2
1	3	2.874	2.87380	1	1	–3
5	9	2.831	2.83159	1	1	3
1	4	2.753	2.75415	3	0	–2
20	16	2.720	2.72093	0	0	4
5	3	2.680	2.68117	3	0	2
25	37	2.647	2.64910	0	2	0
5	3	2.602	2.60301	3	1	1
1	2	2.571	2.57395	0	2	1
10	10	2.549	2.54992	1	2	0
5	7	2.495	2.49657	2	1	3
15	11	2.443	2.44370	3	1	–2
5	3	2.420	2.42040	0	1	4
1	3	2.391	2.39229	3	1	2
1	2	2.351	2.35178	4	0	0
5	9	2.327	2.32860	1	1	4
15	9	2.317	2.31650	1	2	–2
5	6	2.149	2.14953	4	1	0
5	6	2.136	2.13481	4	0	2
10	11	2.019	2.01888	4	1	–2
1	2	1.980	1.98012	4	1	2
1	2	1.908	1.90925	3	2	–2
10	13	1.898	1.89808	0	2	4
10	4	1.883	1.88443	3	2	2
5	3	1.869	1.86844	1	2	–4
1	2	1.792	1.79151	1	0	–6
1	2	1.773	1.77354	2	2	–4
1	2	1.753	1.75257	4	0	4
5	4	1.711	1.71046	4	1	–4
5	4	1.680	1.67961	1	1	6
1	1	1.663	1.66248	1	2	–5
5	5	1.596	1.59717	2	1	6
10	4	1.592	1.59171	3	0	–6
1	5	1.577	1.57718	2	3	2
10	5	1.568	1.56785	6	0	0
5	2	1.563	1.56228	1	3	3
5	5	1.550	1.54945	3	0	6
5	4	1.534	1.53392	5	2	0
5	4	1.506	1.50571	5	1	–4
1	2	1.487	1.48667	3	3	–2
1	2	1.482	1.48138	0	3	4
5	3	1.460	1.45956	1	3	4
1	2	1.349	1.34925	6	2	0
1	2	1.338	1.33747	3	2	6
5	3	1.318	1.31772	0	1	8
1	2	1.310	1.31040	1	1	–8
1	1	1.302	1.30151	6	2	2
5	2	1.300	1.29963	6	1	4
1	2	1.222	1.22185	6	2	–4

I_{cal}, (h,k,l): based on the results of the single-crystal data refinement using VESTA (Momma and Izumi 2011); d_{cal}: derived from unit cell refinement using UnitCell (Holland and Redfern 1997)

d_{obs}, I_{obs}: visually using an ENRAF-NONIUS Gunier viewer, reading accuracy ≈0.03 °2θ

Measurement: Gandolfi camera (Gandolfi 1964) in asymmetric setting, ∅ 114.85 mm, Cu$K\alpha$, Ni-filter, 16 h

banded native arsenic. This matrix is covered by a thin, amorphous film with noticeable shrinkage cracks (Fig. 2). The film is the substrate for stergiouite and well-developed

Table 2 Crystal data and details of the intensity measurement and structure refinement for stergiouite

Crystal data	stergiouite
formula	$CaZn_2(AsO_4)_2 \cdot 4H_2O$
space group	*Pc*
a (Å)	9.416(2)
b (Å)	5.300(1)
c (Å)	10.893(2)
β (°)	91.77(1)
V (Å^3)	543.4(2)
Z	2
ρ_{calc} (g cm^{-3})	3.183
μ (Mo$K\alpha$) (mm^{-1})	10.99
Data collection and refinement	
$2\theta_{max}$ (°)	73
unique data	5298
data with $F_o > 4\sigma(F_o)$	4044
variables / restraints	179 / 16
$R1$ [for $F_o > 4\sigma(F_o)$] [1]	0.0458
$wR2$ [for all F_o^2] [1]	0.0899
a, $b1$	0.041, 1.20
$\Delta\rho_{min\ /\ max}$ (eÅ^{-3})	−1.02 / 3.19

[1] $R1 = \|\|Fo|-|Fc\|\| / |Fo|$; $wR2 = \left[w\left(F_o^2-F_c^2\right)^2 / w\left(F_o^2\right)^2\right]^{\delta}$;

$w = 1/\left[\sigma^2\left(F_o^2\right) + (a \times P)^2 + b \times P\right]$;

$P = \left\{\left[\max \text{ of } \left(0 \text{ or } F_o^2\right)\right] + 2F_c^2\right\}/3$

Table 3 Atomic coordinates and displacement parameters with e.s.d.'s in parentheses for stergiouite

	x	*y*	*z*	$U_{iso/eq}$	U^{11}	U^{22}	U^{33}	U^{23}	U^{13}	U^{12}
Ca	0.0000(2)	0.2425(3)	0.50000(17)	0.0164(2)	0.0208(6)	0.0147(6)	0.0141(5)	−0.0006(5)	0.0038(4)	0.0026(5)
Zn1	0.50429(13)	0.5518(2)	0.40479(10)	0.0132(2)	0.0160(6)	0.0117(5)	0.0120(5)	−0.0006(5)	0.0007(4)	−0.0002(5)
Zn2	0.50640(13)	0.0452(2)	0.60811(10)	0.0134(2)	0.0150(6)	0.0148(5)	0.0102(5)	0.0000(5)	0.0001(4)	0.0011(5)
As1	0.32140(8)	0.03317(18)	0.34731(7)	0.0108(2)	0.0122(5)	0.0100(4)	0.0102(5)	−0.0001(4)	−0.0006(4)	−0.0005(4)
As2	0.69007(9)	0.52358(17)	0.66383(7)	0.0095(2)	0.0073(5)	0.0115(4)	0.0096(4)	0.0003(4)	−0.0002(4)	0.0008(4)
O1	0.3613(7)	0.3390(13)	0.3362(6)	0.0204(14)	0.029(4)	0.005(3)	0.027(3)	0.004(3)	−0.009(3)	−0.007(2)
O3	0.1495(11)	−0.0018(11)	0.3801(10)	0.0173(18)	0.018(5)	0.012(3)	0.022(5)	−0.003(2)	0.008(4)	0.000(2)
O2	0.3533(7)	−0.1180(15)	0.2161(6)	0.0206(14)	0.020(3)	0.025(4)	0.017(3)	−0.006(3)	0.003(2)	−0.009(3)
O4	0.4281(7)	−0.1133(12)	0.4567(5)	0.0156(13)	0.021(3)	0.011(3)	0.014(3)	0.000(2)	−0.004(2)	0.003(3)
O5	0.8591(10)	0.4831(12)	0.6294(9)	0.0156(17)	0.006(4)	0.024(4)	0.017(4)	−0.001(2)	−0.001(3)	0.003(2)
O6	0.6566(7)	0.8336(14)	0.6720(8)	0.0297(19)	0.021(4)	0.010(3)	0.058(5)	−0.003(4)	−0.013(3)	0.002(3)
O7	0.6619(8)	0.3849(16)	0.7988(6)	0.0217(15)	0.023(4)	0.031(4)	0.011(3)	0.007(3)	0.007(2)	0.005(3)
O8	0.5770(7)	0.3862(12)	0.5587(6)	0.0154(13)	0.020(3)	0.014(3)	0.012(3)	0.002(2)	−0.007(2)	−0.006(3)
O9	0.1911(11)	0.4600(17)	0.5911(9)	0.036(2)	0.031(4)	0.040(4)	0.035(4)	−0.009(3)	−0.018(3)	0.005(3)
H9a	0.254(12)	0.40(2)	0.648(9)	0.053						
H9b	0.174(9)	0.624(8)	0.608(11)	0.053						
O10	0.0169(8)	−0.0767(14)	0.6453(6)	0.0281(14)	0.036(4)	0.026(3)	0.022(3)	0.005(3)	−0.002(2)	−0.011(3)
H10a	0.053(13)	−0.05(2)	0.722(5)	0.042						
H10b	−0.030(11)	−0.226(12)	0.649(10)	0.042						
O11	−0.1898(11)	0.0342(15)	0.3971(9)	0.0326(18)	0.031(4)	0.033(4)	0.033(4)	0.000(3)	−0.009(3)	−0.005(3)
H11a	−0.222(12)	−0.124(9)	0.399(12)	0.049						
H11b	−0.242(11)	0.109(19)	0.336(8)	0.049						
O12	0.0018(8)	0.5623(14)	0.3575(6)	0.0273(14)	0.031(3)	0.030(4)	0.020(3)	0.005(3)	−0.008(2)	−0.011(3)
H12a	−0.028(13)	0.544(15)	0.279(4)	0.041						
H12b	0.061(10)	0.699(14)	0.356(9)	0.041						

crystals of native sulfur. In addition, pharmacolite, köttigite, picropharmacolite and hörnesite have been identified.

Stergiouite probably originates from the oxidation of sphalerite and native arsenic and the dissolution of the surrounding calcite. The new mineral is among the latest to form with only native sulfur succeeding in the sequence.

Morphological, physical and optical properties

Morphological features were studied by secondary electron (SE) imaging in a Phenom GSR Desktop scanning electron microscope. Stergiouite occurs as clusters of stacked, thin platy crystals (Fig. 3) overgrown on various other minerals of the assemblage. Individual plates // (100) rarely exceed $200 \times 100 \times 5$ μm^3 in size. Most of the crystals, however, are thinner than 2 μm. The forms {100}, $\{\bar{1}00\}$ are dominant, {010}, {001}, $\{00\bar{1}\}$, {101}, $\{10\bar{1}\}$, $\{\bar{1}0\bar{1}\}$ and $\{\bar{1}01\}$ are subordinate. No twinning was observed; inversion twinning is inferred from the X-ray structure refinement.

Stergiouite exhibits a perfect clevage on {100} and uneven fracture in other directions. The Mohs hardness is ~3 and the tenacity is brittle. The mass density was measured using micro-pycnometry ($CHBr_3$-filled capillary with an inner diameter of 0.5 mm and a length of 10 cm) to be 3.1(2) g cm^{-3}. Considering the limited amount of pure material available for testing, the above value compares well with the calculated mass density of 3.183 g cm^{-3}, based on the empirical formula and unit-cell dimensions obtained from single-crystal X-ray diffraction. The mineral is colorless or white, shows transparent to translucent diaphaneity and has a pearly luster. No luminescence was observed under long-wave and short-wave UV radiation.

Stergiouite is optically biaxial (−). Refractive indices measured at a wavelength of 589 nm are $n_\alpha = 1.561(3)$, $n_\beta = 1.619(3)$; $n_\gamma = 1.621(5)$; $2\ V = 20(1)°$. α is oriented ~ perpendicular to (100) and β is parallel to [010]. Calculating K_c for the empirical formula, using the Gladstone-Dale relationship (Gladstone and Dale 1863) and based on the empirical values of Mandarino (1976), revealed a compatibility index $1 - (K_p/K_c) = 0.01$, which is rated as superior (Mandarino 1981). There is no discernible pleochroism, and the optical dispersion is very weak, with $n_{red} < n_{violet}$.

Table 4 Selected interatomic bond distances (Å) and angles (°) for stergiouite

Ca–O12	2.299(7)	As1–O1	1.669(7)
Ca–O10	2.319(7)	As1–O2	1.674(7)
Ca–O9	2.333(9)	As1–O3	1.679(11)
Ca–O3	2.341(10)	As1–O4	1.719(6)
Ca–O5	2.343(10)	**<As1–O>**	**1.685**
Ca–O11	2.355(9)		
<Ca[6]–O>	**2.332**	O1–As1–O2	110.9(4)
		O1–As1–O3	110.1(3)
Zn1–O1	1.893(7)	O2–As1–O3	109.2(4)
Zn1–O7	1.937(7)	O1–As1–O4	111.1(3)
Zn1–O8	1.995(6)	O2–As1–O4	105.0(3)
Zn1–O4	2.003(6)	O3–As1–O4	110.5(4)
<Zn1–O>	**1.957**	**<O–As1–O>**	**109.47**
O1–Zn1–O7	114.6(3)	As2–O5	1.660(10)
O1–Zn1–O8	106.9(3)	As2–O6	1.676(8)
O7–Zn1–O8	109.1(3)	As2–O7	1.672(7)
O1–Zn1–O4	112.5(3)	As2–O8	1.703(6)
O7–Zn1–O4	107.6(3)	**<As2–O>**	**1.678**
O8–Zn1–O4	105.6(3)		
<O–Zn1–O>	**109.38**	O5–As2–O7	108.7(4)
		O5–As2–O6	108.8(3)
Zn2–O6	1.919(7)	O7–As2–O6	110.4(4)
Zn2–O2	1.927(7)	O5–As2–O8	112.1(4)
Zn2–O4	1.974(6)	O7–As2–O8	106.9(3)
Zn2–O8	2.005(6)	O6–As2–O8	109.9(3)
<Zn2–O>	**1.956**	**<O–As2–O>**	**109.47**
O6–Zn2–O2	116.9(3)	O9–H9a···O2	2.710
O6–Zn2–O4	107.9(3)	O9–H9b···O10	3.021
O2–Zn2–O4	109.2(3)	O10–H10a···O3	2.841
O6–Zn2–O8	112.2(3)	O10–H10b···O5	2.769
O2–Zn2–O8	104.1(3)	O11–H11a···O7	2.817
O4–Zn2–O8	106.1(3)	O11–H11b···O6	2.895
<O–Zn2–O>	**109.40**	O12–H12a···O5	2.799
		O12–H12b···O3	2.704

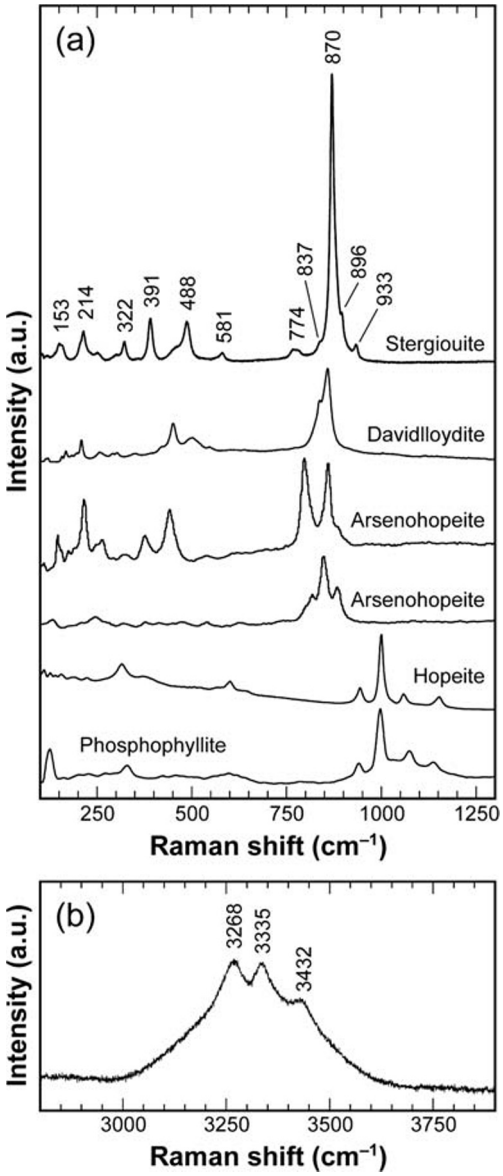

Fig. 4 Raman spectroscopy of stergiouite. **a** The 100–1300 cm^{-1} spectral range is dominated by an intense band at 870 cm^{-1}. Reference spectra were extracted from Hawthorne et al. (2012; davidlloydite), Neuhold et al. (2012; two spectra of arsenohopeite) and Pawlig et al. (2001; hopeite and phosphophyllite). **b** Raman spectrum in the H–O stretching range

Chemical composition

Chemical analyses were performed with a JEOL Hyperprobe JXA8530F electron probe microanalyser (EPMA) equipped with a field-emission electron gun, operated in wavelength-dispersive X-ray spectrometry (WDS) mode. Nine spot analyses were conducted with an accelerating voltage of 10 kV, 20 nA beam current and 30 μm beam diameter. Calibrant materials used (X-ray lines analysed are quoted in brackets) were InAs (As–L_α, Sb_2S_3 (Sb–L_α), wollastonite (Ca–K_α), and ZnO (Zn–K_α). The mean EPMA results (ranges are quoted in brackets) are As_2O_5 42.93 (41.99–43.26) wt%; Sb_2O_5 2.45 (0.0–2.47) wt%; CaO 10.90 (10.85–10.98) wt%; ZnO 29.79 (29.61–30.01) wt%; H_2O 13.81 wt% (calculated from the structure); total 99.88 wt%. The empirical formula (calculated based on 12 O apfu) is $Ca_{1.02}Zn_{1.91}((As_{0.95}Sb_{0.08})O_4)_{\Sigma 2.03} \cdot 4H_2O$. The simplified formula is $CaZn_2(AsO_4)_2 \cdot 4H_2O$, which corresponds to a theoretical composition of CaO 10.76 wt%; ZnO 31.25 wt%; As_2O_5 44.14 wt% and H_2O 13.85 wt%. The mineral was found to be soluble in diluted HCl and in diluted H_2SO_4.

X-ray diffraction analysis

X-ray powder diffraction was done with a Gandolfi camera (Gandolfi 1964) of 114.85 mm diameter, using Cu–$K\alpha$

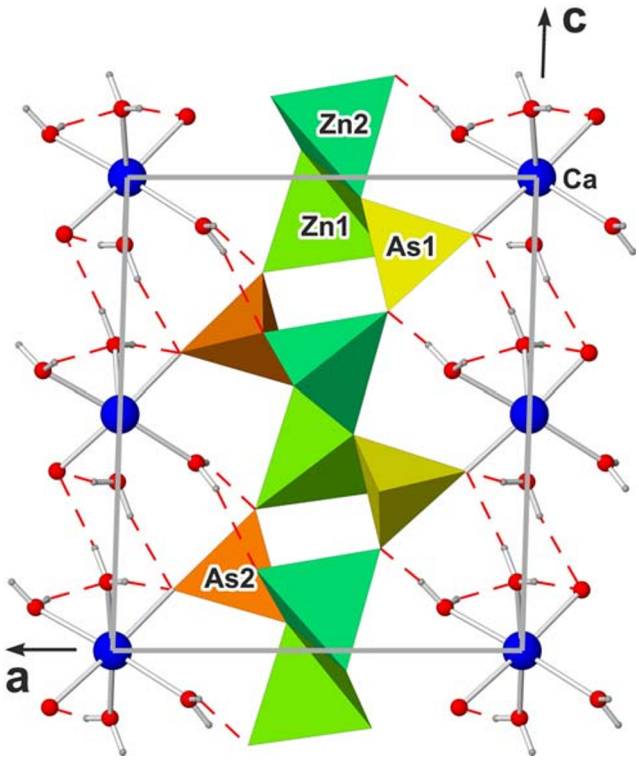

Fig. 5 Structure of stergiouite projected along [010]. All structure drawings were done with the ATOMS software (Dowty 2016)

radiation (Ni filter). The recorded diffraction lines are listed in Table 1. Unit-cell parameters refined from powder data using the UNIT-CELL software (Holland and Redfern 1997) are *a* 9.412(3) Å; *b* 5.298(2) Å; *c* 10.889(3) Å; β 91.78(2)°; *V* 542.7(2) Å^3.

A tiny fragment (0.09 × 0.08 × 0.005 mm^3 in size) was subjected to a single crystal X-ray study. The analysis was done at room temperature on a Bruker Kappa ApexII diffractometer equipped with an Incoatec Microfocus Source IμS (30 W; multilayer mirror; Mo–K_α radiation). Several sets of phi- and omega-scans with 1.5 ° scan width (total 1098 frames; 250 s per frame) were measured with a crystal-detector distance of 40 mm, up to 70 ° 2θ full sphere. A numerical absorption correction was applied. In the centrosymmetric space group $P2_1/c$ no reliable structure model could be established nor was a search in *Pc* indicative for missed symmetry. The crystal structure was solved by direct methods and refined using the Shelx97 software package (Sheldrick 2008) in space group *Pc* to final values of $R1 = 0.046$ and $wR2 = 0.093$. Approximate positions of the H atoms were located and refined with idealized geometry restricting O–H distances to 0.90(2) Å. A compilation of crystal data and details of measurements and refinements are given in Table 2. Note that the single-crystal results are in good agreement with the unit-cell parameters obtained by X-ray powder diffraction. Atomic coordinates and displacement parameters are listed in Table 3, and selected inter-atomic bond distances and bond angles are quoted in Table 4.

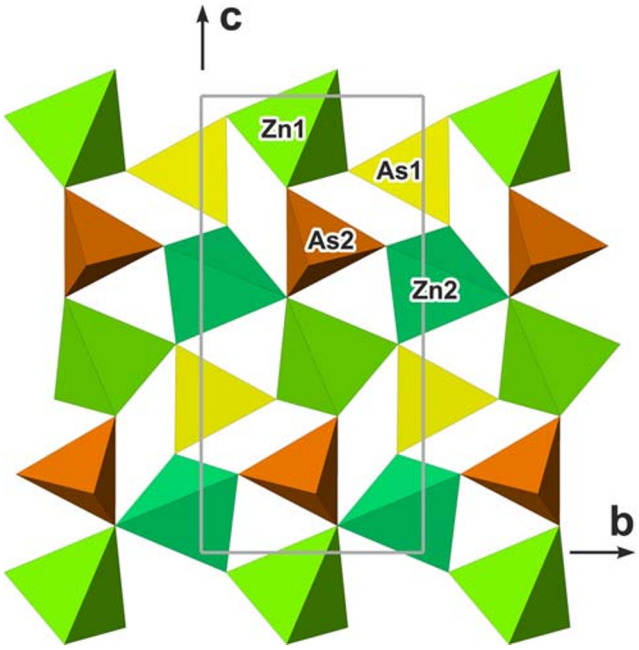

Fig. 6 Tetrahedral layer in the stergiouite structure projected along [100]

Raman spectroscopy

Raman measurements were carried out using a Horiba LabRAM HR Evolution system equipped with Olympus BX41 optical microscope and Si-based, Peltier-cooled charge-coupled device (CCD) detector. An Olympus 50× objective (numerical aperture NA = 0.5) was used to focus the laser beam to the sample surface. Raman spectra were excited with the blue

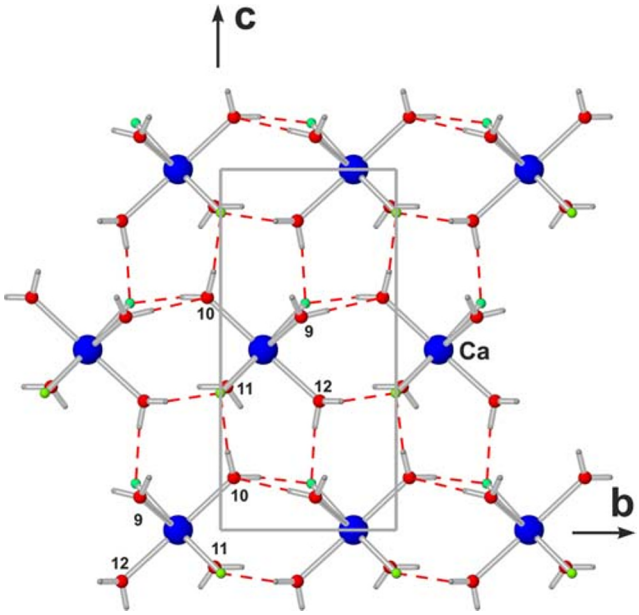

Fig. 7 Octahedral layer in the stergiouite structure projected along [100], illustrating the system of hydrogen bonds within the sheet. Oxygen atoms of H_2O molecules are labelled with numbers

473 nm emission of a diode-pumped solid-state laser (~3 mW at the the sample surface). A grating with 1800 grooves/mm was used to disperse the scattered light, resulting in a spectral resolution of ~1.5 cm^{-1}. The spectrometer was calibrated using the Rayleigh line and Kr-lamp emissions. The wavenumber accuracy was better than 0.5 cm^{-1}. Further analytical details are described elsewhere (Zeug et al. 2018).

The Raman spectrum of stergiouite is shown in Fig. 4. It is dominated by an intense band at 870 cm^{-1}, which is assigned to symmetric stretching vibrations of tetrahedra. Note that in spite of close structural similarities of stergiouite with phosphophyllite and hopeite, the fingerprint patterns of Raman bands show appreciable differences. The spectrum of stergiouite is hence highly indicative of this mineral and makes possible its unambiguous identification. Bands in the 2800–3900 cm^{-1} spectral region are assigned to stretching vibrations of O–H bonds in H_2O molecules. Note that Raman indicates the presence of at least three non-equivalent H_2O species.

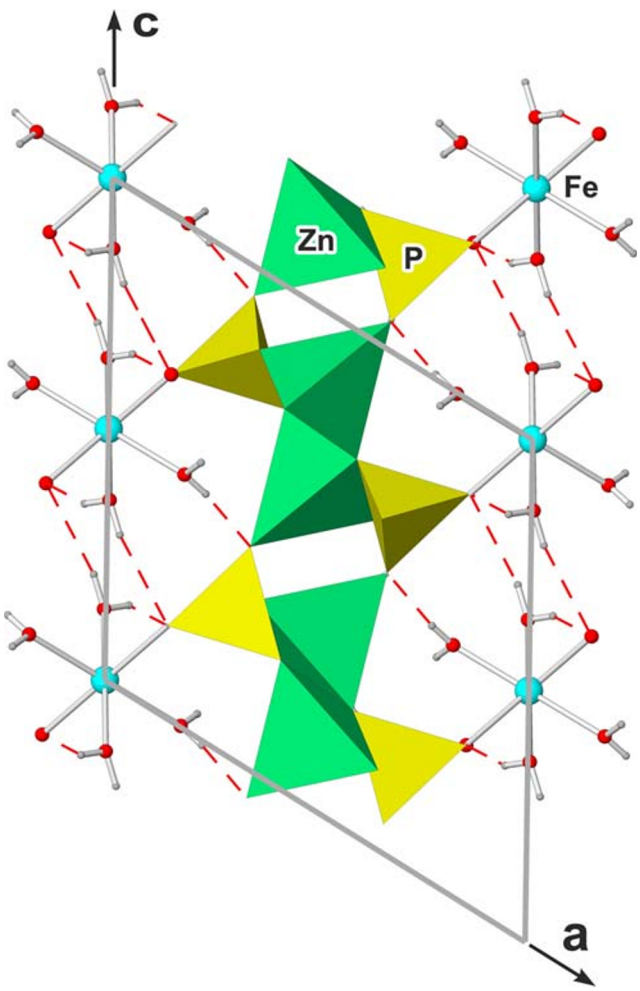

Fig. 8 Structure of phosphophyllite projected along [0$\bar{1}$0]

Discussion

Crystal structure

Stergiouite forms a framework illustrated in Fig. 5. The asymmetric unit contains one $CaO_2(H_2O)_4$ octahedron, two ZnO_4 tetrahedra and two AsO_4 tetrahedra. These tetrahedra share common corners to build a sheet of 3- and 4-membered rings parallel to (100) with ZnO_4 polyhedra centered at x/a ~½ (Figs. 5 and 6). The $CaO_2(H_2O)_4$ octahedra are also arranged in a parallel layer at x/a ~0 (Fig. 7) and linked by two corners with the neighbouring AsO_4 groups. A system of hydrogen bonds (O···O range: 2.70–3.02 Å) further stabilises the structure. Bond distances are 2.30–2.36 Å for Ca–O, 1.89–2.00 Å for Zn1–O, 1.92–2.01 Å for Zn2–O, 1.67–1.72 Å for As1–O and 1.66–1.70 Å for As2–O. Mean bond lengths for $Ca^{[6]}$–O, $Zn^{[4]}$–O and $As^{[4]}$–O comply well with respective values commonly observed for these polyhedra (e.g. Gagné and Hawthorne 2016, 2018).

Related species

Stergiouite is structurally related to phosphophyllite $Fe^{[6]}Zn_2^{[4]}(PO_4)_2 \cdot 4H_2O$ (Laubmann and Steinmetz 1920; Hill 1977; Thomas and Weller 1992). Phosphophyllite was described by Hill (1977) to have

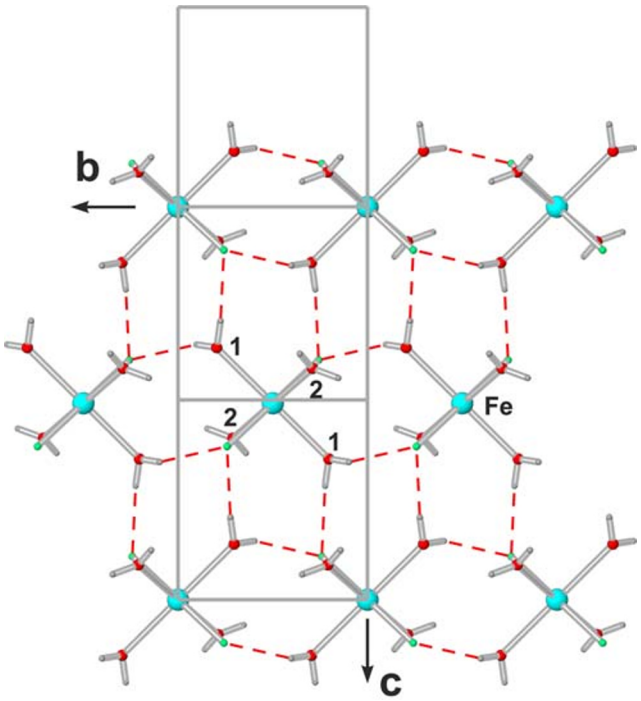

Fig. 9 Octahedral layer in the phosphophyllite structure projected on (100), illustrating the system of hydrogen bonds within the sheet as described by Hill (1977). Oxygen atoms of H_2O molecules are labelled with numbers

space group $P2_1/c$, with a 10.378 Å; b 5.084 Å; c 10.553 Å; β 121.14 °; Z = 2. This mineral is built up by an equivalent sheet of puckered, 3- and 4-membered rings composed of ZnO_4 and PO_4 tetrahedra (see Fig. 8) with intercalated sheets of $FeO_2(H_2O)_4$ octahedra (Fig. 9). Due to the higher symmetry of phosphophyllite compared to stergiouite, the asymmetric unit only consists of one ZnO_4, one PO_4 and one $FeO_2(H_2O)_4$ polyhedron.

The atomic arrangement in the monoclinic minerals stergiouite and phosphophyllite exhibits also clear relationships with orthorhombic members of the hopeite group (8.CA.30 of Nickel-Strunz classification; Strunz and Nickel 2001) that comprises hopeite $Zn^{[6]}Zn_2{}^{[4]}(PO_4)_2 \cdot 4H_2O$ (Hill and Jones 1976), arsenohopeite $Zn^{[6]}Zn_2{}^{[4]}(AsO_4)_2 \cdot 4H_2O$ (Neuhold et al. 2012) and nizamoffite $Mn^{[6]}Zn_2{}^{[4]}(PO_4)_2 \cdot 4H_2O$ (Kampf et al. 2015); all being isotypic in space group *Pnma*. Herschke et al. (2004) have described orthorhombic hopeite in two modifications, both having nearly identical lattice parameters. These include the stable α-hopeite and the metastable β-hopeite; the latter was synthesized at low temperature. The main distinctive features of α- and β-hopeite is the orientation of one of the H_2O molecules.

All of the minerals discussed above have in common that their structures are characterised by topologically corresponding sheets of 3- and 4-membered rings composed of ZnO_4 and XO_4 tetrahedra with X = P, As. As a common feature, the cations M^{2+} = Ca, Mn, Fe, Zn form $MO_2(H_2O)_4$ octahedra situated between the sheets of tetrahedra and linked by two corners to adjacent XO_4 tetrahedra. Differences occur with respect to the individual connection of involved layers (Fig. 10) by the $MO_2(H_2O)_4$ octahedra. As a consequence, the b axis in hopeite is approximately two times larger (18.3 Å) compared to the corresponding a axis in stergiouite (9.4 Å) and the d value for (100) in phosphophyllite (8.9 Å).

In contrast, the structures of the triclinic species parahopeite $Zn^{[6]}Zn_2{}^{[4]}(PO_4)_2 \cdot 4H_2O$ (Chao 1969) and davidlloydite $(Zn,Cu)^{[6]}Zn_2{}^{[4]}(AsO_4)_2 \cdot 4H_2O$ (Hawthorne et al. 2012) deviate appreciably from the minerals discussed above. In parahopeite and davidlloydite, tetrahedra form sheets that are only composed of 4-membered rings (for details and discussion see Hawthorne et al. 2012).

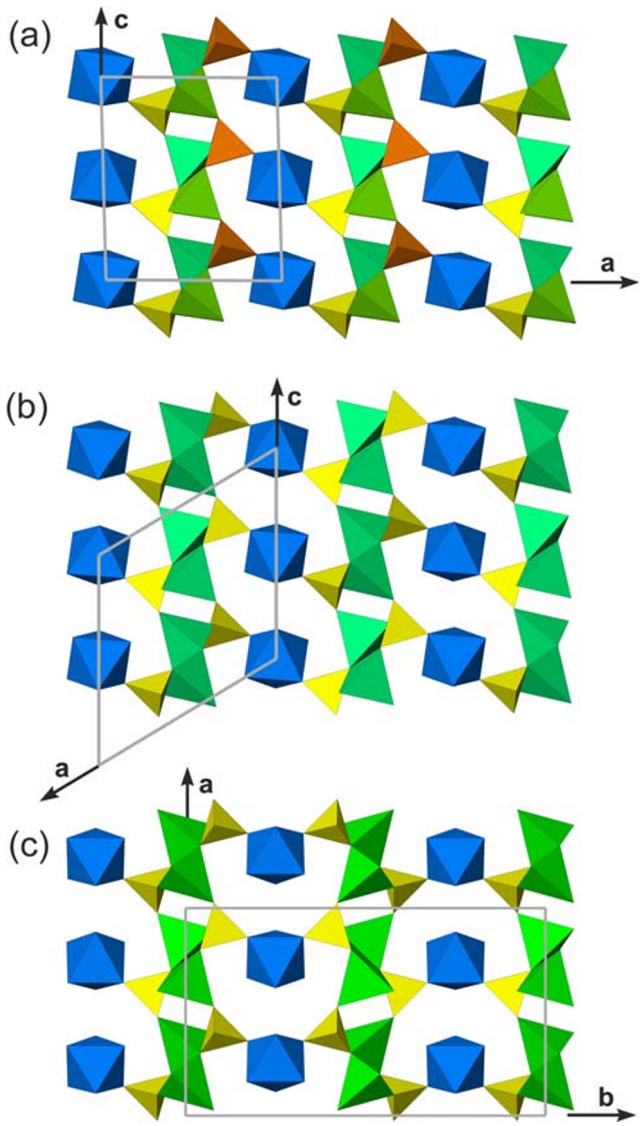

Fig. 10 Arrangement of structural units compared for **a** stergiouite, **b** phosphophyllite and **c** hopeite

Acknowledgements The authors are grateful to Fernando Camera, Anthony R. Kampf and Jakub Plasil for critical and constructive reviews. We thank associate editor Nikita V. Chukanov for corrections and helpful comments that helped to improve the manuscript.

References

Chao GY (1969) Refinement of the crystal structure of parahopeite. Z Kristallogr 130:261–266

Chukanov NV, Pekov I, Belakovskiy DI, Britvin SN, Stergiou V, Voudouris P, Magganas A (2018) Katerinopoulosite, $(NH_4)_2Zn(SO_4)_2 \cdot 6H_2O$, a new mineral from the Esperanza mine, Lavrion, Greece. Eur J Mineral 30:821–826

Conophagos CE (1980) Le Laurium antique et la technique grecque de la production de l'argent. Ekdotike Hellados (National Technical University), Athens, Greece, 458 pp (in French)

Dowty E (2016) Atoms V6.5.0 for atomic structure display. Shape software, 521 Hidden Valley road, Kingsport, TN 37663 USA

Gagné OC, Hawthorne FC (2016) Bond–length distributions for ions bonded to oxygen: alkali and alkaline–earth metals. Acta Crystallogr B 72:602–625

Gagné OC, Hawthorne FC (2018) Bond–length distributions for ions bonded to oxygen: metalloids and post-transition metals. Acta Crystallogr B 74:63–78

Gandolfi G (1964) Metodo per ottenere uno spettro di polveri da un cristallo singolo di piccole dimensioni (fino a 30 μ). Mineral Petrogr Acta 10:149–156

Giester G, Rieck B (1995) Mereiterite, $K_2Fe[SO_4]_2 \cdot 4H_2O$, a new leonite–type mineral from the Lavrion Mining District, Greece. Eur J Mineral 7:559–566

Giester G, Rieck B (2014) Crystal structure refinement of aurichalcite, $(Cu,Zn)_5(CO_3)_2(OH)_6$, from the Lavrion Mining District, Greece. Neues Jb Miner Abh: J Mineral Geochem 191:225–232

Giester G, Rieck B, Brandstätter F (1998) Niedermayrite $Cu_4Cd(SO_4)_2(OH)_6 \cdot 4H_2O$, a new mineral from the Lavrion Mining District, Greece. Mineral Petrol 63:19–34

Giester G, Lengauer CL, Rieck B (2000) The crystal structure of nesquehonite, $MgCO_3 \cdot 3H_2O$, from Lavrion, Greece. Mineral Petrol 70:153–163

Giester G, Kolitsch U, Leverett P, Turner P, Williams PA (2007) The crystal structures of lavendulan, sampleite, and a new polymorph of sampleite. Eur J Mineral 19:75–93

Gladstone JH, Dale TP (1863) Researches on the refraction, dispersion, and sensitiveness of liquids. Phil Trans R Soc London 153:317–343

Hawthorne FC, Cooper MA, Abdu YA, Ball NA, Back ME, Tait KT (2012) Davidlloydite, ideally $Zn_3(AsO_4)_2(H_2O)_4$, a new arsenate mineral from the Tsumeb mine, Otjikoto (Oshikoto) region, Namibia: description and crystal structure. Mineral Mag 76(1):45–57

Herschke L, Enkelmann V, Lieberwirth I, Wegner G (2004) The role of hydrogen bonding in the crystal structures of zinc phosphate hydrates. Chem Eur J 10(11):2795–2803

Hill RJ (1977) The crystal structure of phosphophyllite. Am Mineral 62: 812–817

Hill RJ, Jones JB (1976) The crystal structure of hopeite. Am Mineral 61: 987–995

Holland TJB, Redfern SAT (1997) Unit cell refinement from powder diffraction data: the use of regression diagnostics. Mineral Mag 61:65–77

Kampf AR, Falster AU, Simmons WB, Whitmore RW (2015) Nizamoffite, $Mn^{2+}Zn_2(PO_4)_2(H_2O)_4$, the Mn analogue of hopeite from the Palermo no. 1 pegmatite, North Groton, New Hampshire. Am Mineral 98:1893–1898

Kolitsch U, Giester G (2013) The crystal structure of a new secondary zinc mineral from Lavrion, Greece: $Zn_9(SO_4)_2(OH)_{12}Cl_2 \cdot 6H_2O$. Mitt Österr Mineral Ges 159:74

Kolitsch U, Rieck B, Brandstätter F, Schreiber F, Fabritz KH, Blaß G, Gröbner J (2014a) Neufunde aus dem altem Bergbau und den Schlacken von Lavrion (I). Mineralien-Welt 25:60–75

Kolitsch U, Rieck B, Brandstätter F, Schreiber F, Fabritz KH, Blaß G, Gröbner J (2014b) Neufunde aus dem altem Bergbau und den Schlacken von Lavrion (II). Mineralien-Welt 25:82–95

Kolitsch U, Rieck B, Voudouris P (2015) Mineralogy and genesis of the Lavrion ore deposit: new insights from the study of ore and accessory minerals. Mitt Österr Mineral Ges 161:66

Krause W, Bernhardt HJ, Braithwaite RSW, Kolitsch U, Pritchard R (2006) Kapellasite, $Cu_3Zn(OH)_6Cl_2$, a new mineral from Lavrion, Greece. Mineral Mag 70:329–340

Laubmann H, Steinmetz H (1920) Der Pegmatit von Hagendorf. Z Kristallogr 55:557–570

Mandarino JA (1976) The Gladstone–Dale relationship - part I: derivation of new constants. Can Mineral 14:498–502

Mandarino JA (1981) The Gladstone-Dale relationship: part IV. The compatibility concept and its application. Can Mineral 19:441–450

Momma K, Izumi F (2011) VESTA 3 for three-dimensional visualization of crystal, volumetric and morphology data – V.3.4.3. J Appl Crystallogr 44:1272–1276

Neubauer F (2005) Structural control of mineralization in metamorphic core complexes. In: Mao J, Bierlein FP (eds) Mineral deposit research: meeting the global challenge. Springer, Berlin, pp 561–564

Neuhold F, Kolitsch U, Bernhardt HJ, Lengauer CL (2012) Arsenohopeite, a new zinc arsenate mineral from the Tsumeb mine, Namibia. Mineral Mag 76(3):603–612

Pawlig O, Schellenschläger V, Lutz HD, Trettin R (2001) Vibrational analysis of iron and zinc phosphate conversion coating constituents. Spectrochim Acta A 57:581–590

Rieck B (1999) Seltene Arsenate aus der Kamariza und weitere Neufunde. Lapis 24(7/8):68–76

Rieck B (2012) Neue Minerale aus dem Lagerstätten-Bezirk Lavrion/Griechenland und den Kalahari Mangan Feldern/Republik Südafrika. PhD Thesis, University of Vienna, 183 pp

Rieck B, Rieck P (1999) Silber, Arsen und Antimon: Vererzungen im Revier Plaka (Teil II). Lapis 24(7/8):59–63

Rieck B, Wendel W (1999) Sounion - Hilarion Top aktuell: Funde vom Frühjahr '99. Lapis 24(7/8):77–78

Rieck B, Kolitsch U, Voudouris P, Giester G, Tzeferis P (2018) Weitere Neufunde aus Lavrion, Griechenland. Mineralien-Welt 29(5):32–77

Rieck B, Lengauer CL, Giester G (2019) Voudourisite, $Cd(SO_4) \cdot H_2O$, and lazaridisite, $Cd_3(SO_4)_3 \cdot 8H_2O$, two new minerals from the Lavrion Mining District, Greece. Mineral Mag 83:551–559

Sheldrick GM (2008) A short history of SHELX. Acta Crystallogr A64: 112–122

Skarpelis N (2002) Geodynamics and evolution of the Miocene mineralization in the Cycladic-Pelagonian belt, Hellenides. Bull Geol Soc Greece 34:2191–2209

Strunz H, Nickel EH (2001) Strunz mineralogical tables. 9th edn. E. Schweitzerbart'sche Verlagsbuchhandlung (Nägele und Obermiller), Stuttgart. ISBN 978-51-6518-7

Thomas IA, Weller MT (1992) Synthesis, structure and thermal properties of phosphophyllite, $Zn_2Fe(PO_4)_2 \cdot 4H_2O$. J Mater Chem 2:1123–1126

Tombros SF, Seymour KS, Spry P (2004) Description and conditions of formation of new unnamed Ag–Cu and Ag–Cu–Au sulfotellurides in epithermal polymetallic Ag–Au–Te mineralization, Tinos Island, Hellas. Neues Jb Miner Abh 179:295–310

Tombros SF, Seymour K, Williams-Jones AE, Spry P (2007) The genesis of epithermal Au–Ag–Te mineralization, Panormos Bay, Tinos Island, Cyclades, Greece. Econ Geol 102:1269–1294

Vavelidis M (1997) Au–bearing quartz veins and placer gold on Sifnos Island, Aegean Sea, Greece. In: Papunen H (ed) mineral deposits: research and exploration - where do they meet? Balkema, pp 335–338

Voudouris P (2005) Gold and silver mineralogy of the Lavrion deposit Attika/Greece. In: Mao J, Bierlein FP (eds) Mineral deposit research: meeting the global challenge. Springer, Berlin Heidelberg, pp 1089–1092

Wendel W, Rieck B (1999a) Die wichtigsten Mineralfundstellen Lavrions. Lapis 24(7/8):25–33

Wendel W, Rieck B (1999b) Silber, Arsen und Antimon: Vererzungen im Revier Plaka (Teil I). Lapis 24(7/8):53–58

Zeug M, Nasdala L, Wanthanachaisaeng B, Balmer WA, Corfu F, Wildner M (2018) Blue zircon from Ratanakiri, Cambodia. J Gemmol 36(2):112–132